Biol. Cybern. 91, 168–181 (2004)
DOI 10.1007/s00422-004-0490-6

Biological Cybernetics

Tactile efficiency of insect antennae with two hinge joints

Andre F. Krause, Volker Dürr

Abt. Biologische Kybernetik und Theoretische Biologie, Fakultät für Biologie, Universität Bielefeld, Postfach 100131, 33501 Bielefeld, Germany

Received: 17 March 2004 / Accepted: 13 May 2004 / Published online: 10 September 2004

Abstract. Antennae are the main organs of the arthropod tactile sense. In contrast to other senses that are capable of retrieving spatial information, e.g. vision, spatial sampling of tactile information requires active movement of the sense organ. For a quantitative analysis of basic principles of active tactile sensing, we use a generic model of arbitrary antennae with two hinge joints (revolute joints). This kind of antenna is typical for Orthoptera and Phasmatodea, i.e. insect orders that contain model species for the study of antennal movements, including cricket, locust and stick insect. First, we analyse the significance of morphological properties on workspace and sampling acuity. It is shown how joint axis orientation determines areas out of reach while affecting acuity in the areas within reach. Second, we assume a parametric set of movement strategies, based on empirical data on the stick insect *Carausius morosus*, and investigate the role of each strategy parameter on tactile sampling performance. A stochastic environment is used to measure sampling density, and a viscous friction model is assumed to introduce energy consumption and, thus, a measure of tactile efficiency. Up to a saturation level, sampling density is proportional to the range or frequency of joint angle modulation. The effect of phase shift is strong if joint angle modulation frequencies are equal, but diminishes for other frequency ratios. Speed of forward progression influences the optimal choice of movement strategy. Finally, for an analysis of environmental effects on tactile performance, we show how efficiency depends on predominant edge direction. For example, with slanted and non-orthogonal joint axis orientations, as present in the stick insect, the optimal sampling strategy is less sensitive to a change from horizontal to vertical edge predominance than with orthogonal and non-slanted joint axes, as present in a cricket.

Electronic Supplementary Material Supplementary material is available in the online version of this article at http://dx.doi.org/10.1007/s00422-004-0490-6

Correspondence to: A. Krause
(e-mail: post@andre-krause.net)

1 Introduction

Many animals use vision for the perception of objects in their environment, but other cues, like auditory or tactile information, are used as well. Insects and crustaceans, for example, use their antennae for wall-following (Camhi and Johnson 1999) and tactile obstacle detection (Pelletier and McLeod 1994; Zeil et al. 2001). In the latter cases, antennae are employed as active tactile sensors that sample the space immediately in front of the animal.

Insect antennae carry sensory hairs of several modalities, including chemo-, mechano-, thermo-, and hygroreceptive hairs, and therefore act as receivers of various external signals, such as surface information about the touched object. Furthermore, insects can direct the sensory receptive fields of these receivers by means of active movement, allowing active exploration of the surrounding space (e.g. Dürr et al. 2001) and tracking of external objects (e.g. Honegger 1981).

Compared to other sensory systems, the active sense of touch, particularly the tactile sense of the antennae, is very little understood. This is reflected by the fact that fundamental considerations about the principles that determine workspace and sensory resolution are lacking. Yet the diversity of insect antennae, both morphological and in terms of movement strategy, suggests that the varied parameters have a differential effect on competing objectives in sensory performance of the antennae. To understand the functional significance of different antennal shapes and different ways to move an antenna, it is desirable to understand the relationship between the mechanics and kinematics of an antenna and its sampling efficiency. This will help us to link the functional properties of the tactile sense to evolutionary trends and also to apply concepts of active tactile sensing in biomimetic sensory devices. An example where such a physics-based approach has proved to be of great importance to the understanding of sensory function is the impact of various construction features of compound eyes on their optical resolution and light sensitivity (e.g. Land 1981; Warrant and McIntyre 1993).

The antennae of pterygote (winged) insects have three functional segments (Imms 1939): the two proximal segments, called scape and pedicel, are articulated and actively moveable while the distal segment, the flagellum, consists of many annuli, which are only passively movable. In particular, the flagellum is equipped with sensory hairs of various modalities (for review see Staudacher et al. 2004, in press) that probe the mechanical characteristics of objects. Proprioreceptors on and inside the scape and pedicel signal the position and movement of the antenna.

Although many insect species share these basic 'construction principles' of their antennae, i.e. three functional segments connected by two joints, morphological parameters such as the joint axis orientation or segment lengths and particularly the movement strategies vary considerably between species. Whereas the scape–pedicel joint is always a hinge joint with a single degree of freedom, the complexity of the head–scape joint varies between species. For example, the head–scape joint of bees, ants and cockroaches is a ball-and-socket joint that allows higher dexterity than a hinge joint as it is found in locusts, crickets and stick insects. Here, we restrict our analysis to the latter case, where both the head–scape and the scape–pedicel joint are hinge joints.

This two-hinge-joint construction is commonly found in the orders Orthoptera and Phasmatodea and includes many species that are known to employ their antennae in active tactile sensing. For example, stick insects and crickets continuously move their antennae during walking (Horseman et al. 1997; Dürr et al. 2001). The antennae perform a rhythmic movement pattern that is temporally coupled to the stepping rhythm of the front legs (Dürr et al. 2001). Such active movements allow a nearly one-dimensional sensor to sample a three-dimensional (3D) volume. Furthermore, stick insects use antennal tactile cues to trigger body axis inclination when climbing over obstacles (Dürr et al. 2003).

Here we employ a generic model of arbitrary antennae to study active antennal movements to quantify the effects of various morphological parameters and movement strategies on the sampling efficiency of the antennae. First, the impact of morphology on the workspace and its relation to sampling resolution of the antennae is analysed. For example, in crickets, the hinge joint axes are aligned parallel to the vertical and horizontal planes of the body coordinate system, whereas in stick insects the axes are slanted relative to these planes. In a second step, we use a simple antenna morphology and the morphology of the stick insect *C. morosus* to examine the tactile efficiency of various movement strategies under different environmental conditions.

2 Simulation method

2.1 Antennal kinematics

For simulation experiments, the forward kinematics of an arbitrary two-joint insect antenna (Fig. 1) was calculated as outlined in Appendix A. The antennal morphology is defined by describing axis orientations using ZXY Euler angles and two-segment vectors. Table 1 shows the parameter values of the two standard morphologies, referred throughout the text as 'simple morphology' (Fig. 2a) and '*C. morosus* morphology' (Fig. 2b).

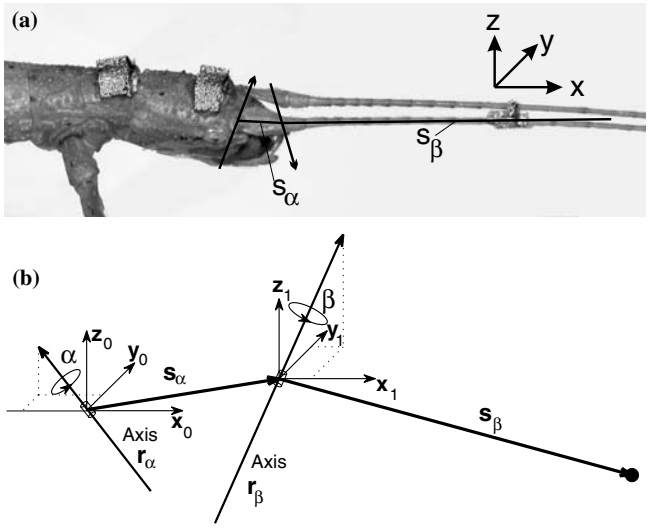

Fig. 1a, b. Construction of a stick insect antenna and conventions for a generic model of an antenna with two hinge joints. **a** Head and antennae of a stick insect of the species *C. morosus*, marked with pieces of retro-reflective foil. **b** General kinematic model of an antenna with two hinge joints. The base frame is located in the head–antenna connection, i.e. the head–scape joint. The x_0-axis of the base frame is aligned with the body long axis, and the z_0-axis points upwards (dorsal). Together with the y_0-axis, a right-hand coordinate system is formed. A rotation around the r_α-axis models the axis of the head–scape joint; the subsequent translation along the first segment, s_α, defines the orientation of the first segment, the scape. A second rotation around the r_β-axis models the motion of the scape–pedicel joint, and a second translation along s_β (pedicel and flagellum) yields the position of the antennal tip. Axis orientations are defined using Euler angles (Table 1)

All calculations were implemented in a custom-written C++ program (Microsoft Visual C++) and visualised with the graphics library OpenGL. Visual display features of the program included special 3D graphs to aid the analysis of a given parameter's impact on the antennal working range or its movement trajectory. For example, the working range of the antenna is illustrated as the envelope that is in reach of the antennal tip, and antennal movements are visualised by means of a ribbon dragged by the flagellum.

Figure 2 shows a visualisation of the two antenna morphologies used in the present study. Arbitrary antennal morphologies could be loaded from parameter files, and additionally all parameters could be modified manually via a graphics interface. A demo version of the simulation software is available from the supplementary material. Adjustable morphology parameters were the segment lengths, the orientation vectors of the segments and joint axes, and the joint angle action ranges.

To simplify the interpretation of simulation results, the unit length in the simulation was set to 1 mm. This also allowed usage of morphological data from the literature, e.g. of the stick insect *C. morosus* (Dürr and Krause 2001), without rescaling.

Table 1. Axis orientation (Euler angles), joint action ranges and segment lengths for the simple and the *C. morosus* morphology (left antenna)

Morphology	Simple		*C. morosus*	
	ϕ	ψ	ϕ	ψ
α-axis	0°	0°	−10°	149°
β-axis	0°	90°	0°	59°
	Offset	Range	Offset	Range
α-axis	0°	90°	50°	100°
β-axis	0°	90°	−40°	80°
	Length		Length	
Scape	0		1.2	
Flagellum	30.0		28.8	

The *C. morosus* morphology models a stick insect antenna, after Dürr and Krause (2001). Segments are perpendicular on the axes. The simple morphology has the same joint axis orientations as a cricket (e.g. *Gryllus campestris*) but an 'ideal' scape of length zero

2.2 Antennal movements

To obtain a biologically sound model of antennal movements, sample trajectories of walking stick insects were analysed using a general solution to the inverse kinematics of an antenna with two hinge joints (Appendix B).

Resulting time courses of antennal joint angles were transformed into the frequency domain, using a fast Fourier transform algorithm (MathCad, MathSoft, Inc.). The complex-valued Fourier coefficients were sorted in descending order according to their magnitude. Reconstructed trajectories were based on linear combinations of the most prominent modes of the frequency spectrum, i.e. the longest coefficient vectors, and evaluated by means of a relative approximation error, as defined in Sect. 3.2.

The results suggest that active movements of the antenna can be simulated by sinusoidal modulation of both joint angles according to the equation

$$\alpha_t = \text{offset}_\alpha + 0.5\,\text{range}_\alpha \sin(2\pi f_\alpha t + \varphi_\alpha)\,,$$

where f_α is the joint angle modulation frequency and φ_α is the phase offset. range_α defines the amplitude of the modulation and offset_α the resting position of the joint.

2.3 Stochastic environmental model

Different antennal morphologies and movement patterns were evaluated in a virtual environment that consisted of a cloud of objects moving toward the antenna at constant speed. A stochastic environment was chosen as it allowed systematic assessment of the impact of a given parameter, e.g. a predominant edge orientation of the objects, on tactile sampling success. The constant speed of the objects simulated constant forward locomotion of the animal within the environment. Size, shape, number and velocity of the objects could be specified. The objects were generated at a random position within a para-frontal plane

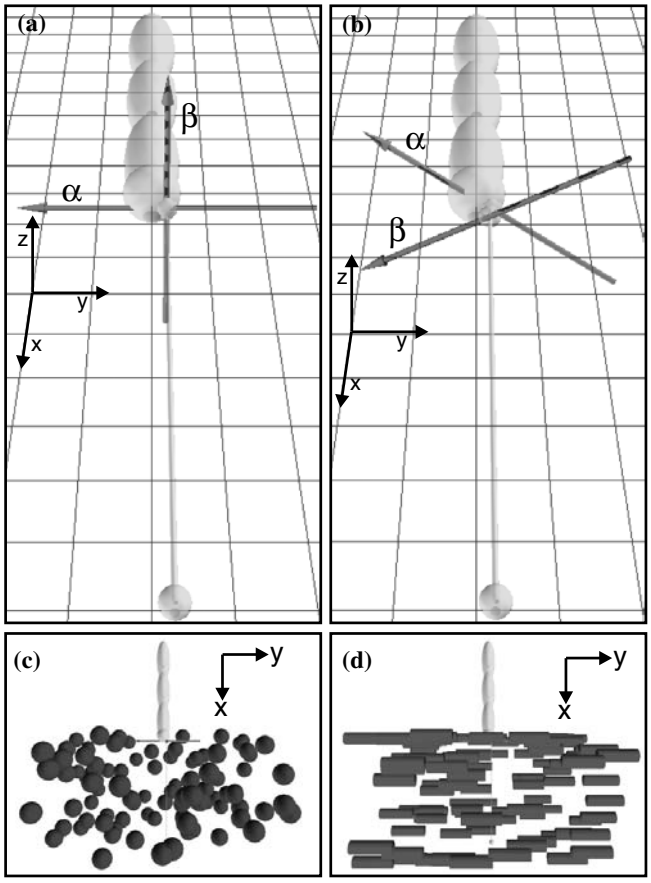

Fig. 2a–d. The two standard antennal morphologies and environments as used in the simulation experiments. The animation shows a cylindrical body, two-joint axes (*arrows*) and the antennal segments, i.e. a very short scape and a long straight pedicel/flagellum with a sphere at its tip. **a** Dorso-frontal view of the 'simple morphology': joint axes are perpendicular to each other and aligned with the axes of the base frame. The first segment has length zero. This arrangement is equivalent to a Cardan joint. **b** '*C. morosus* morphology' after Dürr and Krause (2001). **c** Top view of sphere environment. **d** Top view of cylinder environment. Here, the long axes of the cylinders are parallel to the *y*-axis of the base frame

(Y_0Z_0 plane in Fig. 1 at a distance equal to the length of the antenna ($x = |\mathbf{s}_0| + |\mathbf{s}_1|$).

If an object passed the baseline of the antenna ($x_0 = 0$), it was removed and a new object was generated. Thus, the number of objects (100) in the sampling volume, i.e. the object density, was kept constant. The speed of the objects was set to 50 mm/s, corresponding to the mean walking speed of stick insects on flat surfaces (Kindermann 2003). The motion of the objects was calculated using Euler integration with a constant time step of 20 ms, resulting in a time resolution of the simulation of 50 Hz. Two types of objects were used: (1) spheres with a radius of 2.5 mm and (2) cylinders with a radius of 1.5 mm and a length of 9.26 mm. Thus, cylinders and spheres had identical volumes. The cylinders were aligned parallel to each other and inclined with a constant angle relative to the horizontal plane, i.e. the y_0-axis of the base frame. This allowed systematic introduction of a directional bias.

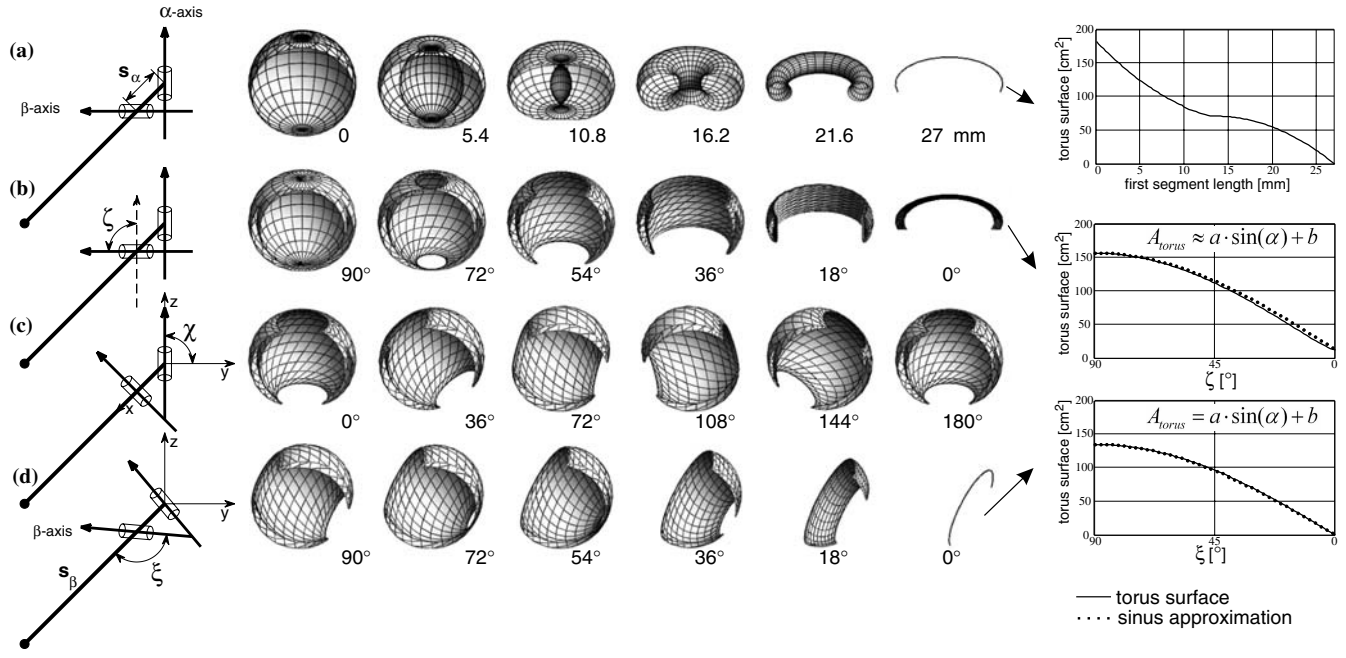

Fig. 3a–d. Influence of various morphological parameters on the antennal workspace. For each row, a given parameter is varied, as indicated by the *inserts* on the *left* (*cylinders* depict hinge joints). For illustration purposes, the shapes indicate the fictive workspace for a complete 360° revolution around both joints. Beginning with the simple morphology of a Cardan joint (*top left*), i.e. orthogonal joint axes, orthogonal segments and an 'ideal' scape of length zero, each row shows the impact of one parameter on the antennal workspace. **a** Variation of the relative length of the first segment, while keeping the total length of the antenna constant ($s_\alpha + s_\beta = 30$ mm, $s_\alpha = 0$ to 30 mm), creates a torus with increasingly narrow range. **b** Variation of the angle between α-axis and β-axis from $\zeta = 90$ to 0° narrows the torus, reducing the surface that can be reached by the antennal tip. Moreover, the torus holes, i.e. out-of-reach zones, become wider. **c** Rotation of the α-axis from 0 to 90° around the x_0-axis of the base frame rotates the entire torus, thus orienting the sampling volume toward a particular region with respect to the animal. The torus itself remains unchanged. **d** Variation of the angle between β-axis and segment 2 from $\xi = 90$ to 0°. The area out of reach widens on one side and narrows on the other. The graphs to the *right* show the dependence of the torus surface on the parameter varied (for details see text)

Antennal contacts with the objects were determined by calculating the putative intersection of each object with the flagellum, assuming a stiff and approximately straight flagellum, as is the case in stick insects. Newly detected contacts were summed up as a hit count variable. Dividing this hit count by the overall number of objects generated gave the relative hit count. For visual supervision of the simulation, detected objects were labelled by a change in colour. Once contacted, objects were excluded from further evaluation.

3 Results

Antennal movements are affected by two major aspects: first, the morphological properties, characterised by segment lengths, joint axis orientation and joint action range, determine the overall working range of the antenna and tactile acuity. Second, the motor physiology and movement strategy, characterised by the muscle-driven movements of the hinge joints, determine the tactile sampling efficiency under different environmental conditions.

3.1 Workspace

To study the impact of the antennal morphology on angular resolution and sampling volume, i.e. the 3D workspace of the flagellum, each morphological parameter was varied at a time, with all others kept constant. Figure 3 shows the influence of a given morphological parameter on the workspace of the antenna. To give an intuitive impression of how the overall workspace features are affected, both joints were considered unconstrained, i.e. allowed complete rotation of 360°. The warped area depicts all possible locations of the antennal tip and, thus, comprises the sampling volume of the antenna. Assuming limited angular precision of the antennal joints, there is a finite number of discernible antennal postures. Accordingly, the surface of the sampling volume is a measure for the area that can be sampled by this finite number of postures. Thus, the surface area of the sampling volume is inversely related to the spatial sampling resolution (see graphs to the right of Fig. 3).

An antenna of the 'simple morphology', i.e. with orthogonal joint axes, orthogonal joint segments and a first segment of length zero, has a spherical workspace identical to the workspace of a Cardan joint (Fig. 3a, left). Increasing the relative length of the first segment leads to a torus-like workspace with an inner and outer surface (Fig. 3a). The torus surface declines monotonically with increasing s_α, with a saddle point where s_α is approximately half the total length.

Reducing the angle ζ between the two joint axes from 90 to 0° compresses the torus-shaped workspace (Fig. 3b).

For short first segments, the torus surface A_{torus} is proportional to $\sin(\zeta)$. For example, $A_{\text{torus}} \approx a \times \sin(\zeta) + b$ for the given example, with $|s_\alpha| = 2\,\text{mm}$, $a = 144.2\,\text{cm}^2$ and $b = 12.5\,\text{cm}^2$.

Rotation of the first axis around the body long axis, i.e. x_0-axis of the base coordinate frame, rotates the whole torus without influencing its shape or volume (Fig. 3c). This is because the torus is axially symmetric around the α-axis. Thus, the orientation of the α-axis determines the location of the holes in the workspace.

Slanting the second segment, i.e. the flagellum, by angle ξ relative to the β-axis introduces an asymmetry that widens the torus on one side and narrows it on the other (Fig. 3d). The torus surface here is always proportional to the sine of ξ, $A_{\text{torus}} = a \times \sin(\xi)$, with $a = 134.5\,\text{cm}^2$.

Because these holes of the torus represent regions that are out of reach for the antenna, appropriate parameter selection allows optimal alignment of the torus-like workspaces: the inter-axis angle and slanting angle of the flagellum determine the width of the out-of-reach zones, whereas the orientation of the head–scape joint determines the location of these zones. Furthermore, assuming limited angular resolution in both joints, a reduction of the workspace increases the positioning accuracy of the flagellum. This is because the same number of 'distinguishable postures' is confined to a narrower range. Finally, as insects carry two antennae, the orientation and shape of the torus also determine the overlap of the two mirror-symmetrical workspaces. For example, an asymmetry that widens the medial out-of-reach zone but narrows the lateral one may reduce medial overlap while optimally sampling the frontal and lateral region around the animal with high accuracy.

In Dürr et al. (2001), segments were assumed to be perpendicular to the axes and only axis orientations were measured. Comparing the resulting workspace of *C. morosus* morphology after Dürr et al. (2001) with antennal trajectories as measured by Dürr et al. (2001) shows that a small fraction of trajectory points are located in the lower out-of-reach area of the workspace torus. Slanting the flagellum by just 12° deforms the torus in such a way that all trajectory points lie within the torus workspace. Additionally, calculation of the inverse kinematics of the 3D trajectories shows that the joint action ranges are reduced significantly, suggesting that *C. morosus* indeed has a slanted flagellum. Figure 4a shows the unconstrained workspace of a *C. morosus* morphology with a flagellum slanted by 12°. Note the asymmetry narrowing the lower left torus hole. This makes the antenna more suitable for sampling the left hemisphere of the insect.

To obtain an estimate of the physical constraints on each antennal joint of a *C. morosus* antenna, cuticular structures of antennal segments and of the head capsule were reconstructed from cross-section slices and rotated around the condyli (Fig. 4b). Maximum possible joint action ranges were then estimated from the 3D reconstruction by visually judging the hard stops, i.e. if cuticular structures penetrate each other (ignoring limits such as max. muscle fiber lengths). These action ranges are larger than joint action ranges calculated from experimental trajectory data (Fig. 5, using inverse kinematics as outlined in Appendix B), suggesting that stick insects use an action range considerably smaller than would be possible considering only cuticular structures.

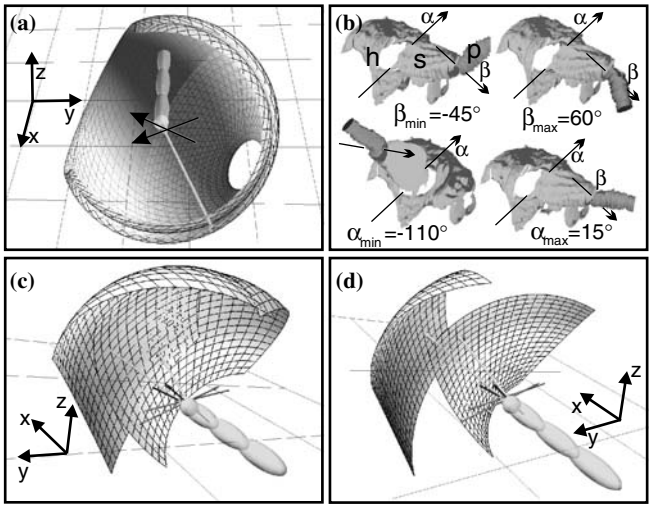

Fig. 4a–d. Workspace of a stick insect antenna. *Arrows* show the orientation of the two hinge joint axes. The torus-like workspace of the antennal tip marks the outer envelope of the volume that can be sampled with the antenna. **a** Workspace of a *C. morosus* antenna, visualised using a joint angle action range of 360° for both joints. The workspace is cut open along a para-frontal plane. **b** Joint angle limits estimated from a 3D reconstruction of cuticular structures of the head (h), the scape (s) and the pedicel (p). *Top*: maximal adduction (β_{min}) and abduction (β_{max}) of the pedicel. *Bottom*: maximal levation (α_{min}) and depression (α_{max}) of the scape. **c** Workspace of a pair of *C. morosus* antennae using joint limits from **b**. Note the overlap in the centre. **d** Workspace using joint limits estimated from experimental trajectories of Dürr et al. (2001), using inverse kinematics (Fig. 5). The overlap is now smaller

3.2 Active movements

To model different movement strategies in a systematic way, we based the set of tested strategies on properties of empirical trajectories. To date, the stick insect is the only insect for which behavioural data on unrestrained 3D antennal movements are available. The stick insect *C. morosus* continuously moves its antennae during walking (Dürr et al. 2001) (Fig. 5a, b). The movement pattern is periodical and temporally coupled to the step cycle of the front legs. During a single front leg step, the ipsilateral antenna executes one abduction/adduction cycle (horizontal excursion) and approximately two levation/depression cycles (vertical excursions). Due to the lack of an inverse kinematics solution, Dürr et al. (2001) did not calculate the time courses of actual joint angles but only the orientation of the flagellum relative to the body coordinate system. A general solution to the inverse kinematics problem of an insect antenna with two hinge joints is given in Appendix B. Application of this solution to original data from Dürr et al. (2001) gives pairs of complex, quasi-periodic joint angle time courses (e.g. Fig. 5c). To model these joint movements, we propose sinusoidal modulation of joint angles.

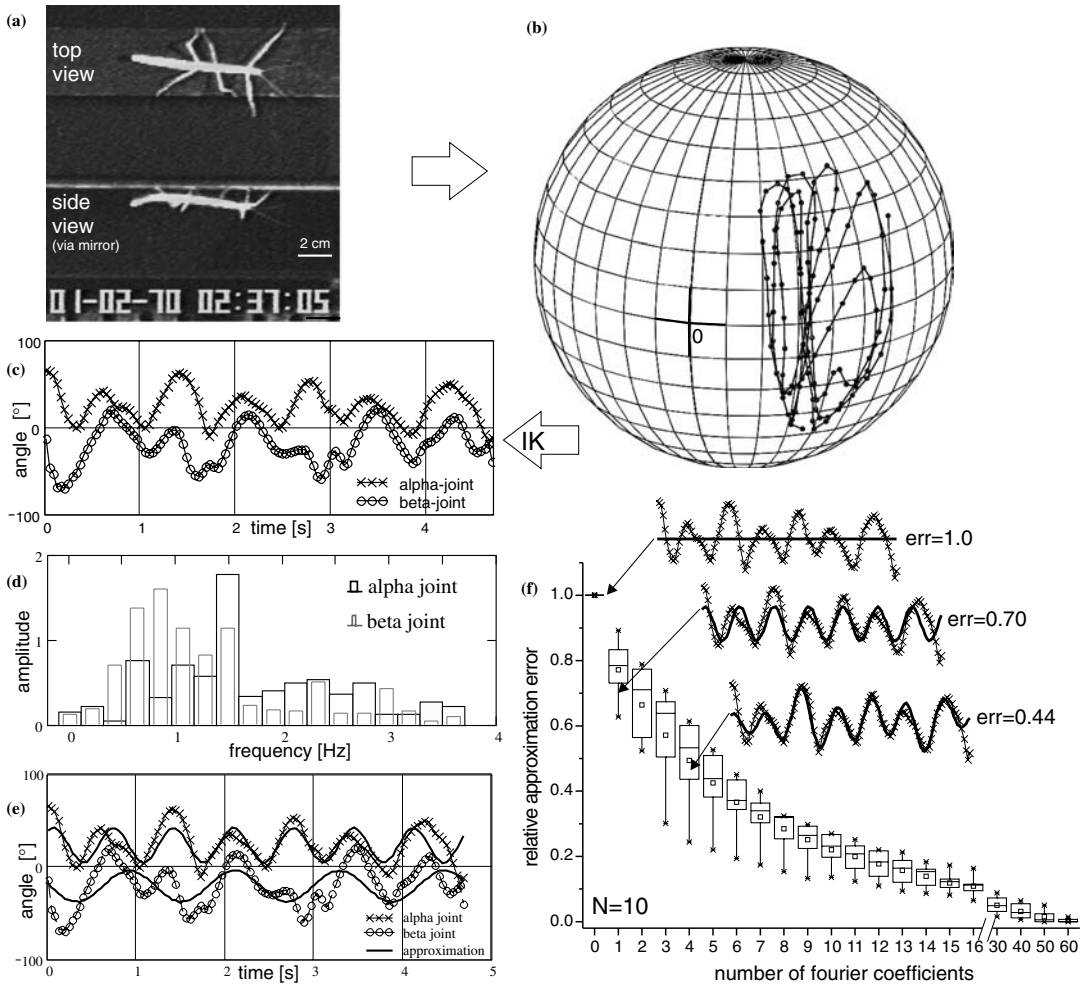

Fig. 5. Analysis of antennal trajectories of unconstrained walking stick insects. Inverse kinematics and Fourier analysis reveal that sinusiodal modulation of joint angles is an appropriate model for an antennal movement strategy. **a** Antennal movements of a freely walking stick insect can be measured from video recordings with top and side view of a stick insect walking along a flat bridge. **b** Polar plot of a sample trajectory of the antennal tip, taken from Dürr et al. (2001), showing azimuth and elevation of the antennal tip in a head-centred coordinate system. The *cross* marks the longitudinal axis of the insect (x_0-axis). **c** Joint angles calculated using inverse kinematics, according to Appendix B: head–scape joint (*crosses*) and scape–pedicel joint (*circles*). **d** Transformation of the joint angles into frequency domain, using Fourier analysis. Head-scape joint (*grey bars*) and scape-pedicel joint (*white bars*). The peaks of the dominant frequencies differ between the joint axes, here with a higher frequency for the α-joint than for the β-joint. **e** The dominant frequencies from **d** give a simple but reasonable approximation of the joint angle trajectories, reflecting the main mode of the movement. **f** If multiple frequencies are used to reconstruct the joint angle trajectories, approximation errors can be reduced. The relative approximation error for the head–scape joint, depending on the number of Fourier coefficients used, is shown ($n = 10$ trajectories from four animals)

A more detailed analysis using Fourier transform of the joint angle trajectories into frequency domain shows that the frequency spectrum of each joint is dominated by a single mode. Using only the main frequency of this mode, i.e. the largest Fourier coefficient, allows reasonable approximation of the joint angle time courses (e.g. the α joint angle as shown in Fig. 5e). Figure 5f shows that adding more coefficients to the reconstruction of the time course causes only slow further reduction of the approximation error. The complex-valued Fourier coefficients are sorted in descending order according to magnitude. The relative approximation error is defined as the summed angular deviations for all frames of the video analysis divided by the maximum possible deviation from the original data, i.e. a flat line located at the median.

3.2.1 Single-joint antenna. To obtain first insights into the impact of active movements on the tactile sampling efficiency of an antenna, a single-joint antenna was moved within the sphere environment. In this simple case, two parameters influence the relative hit count of the single-joint antenna: (1) the joint angle modulation frequency and (2) the action range of the joint. When increasing the joint action range from 0 to 180°, while keeping the joint angle modulation frequency constant at 1 Hz, the relative hit count shows a sine-shaped dependence on the action range (Fig. 6). This is because the length of the projection of the flagellum vector into the frontal (YZ-)plane increases with the sine of half of the action range. Up to an action range of 90° the dependence of the hit count on the action range is nearly linear.

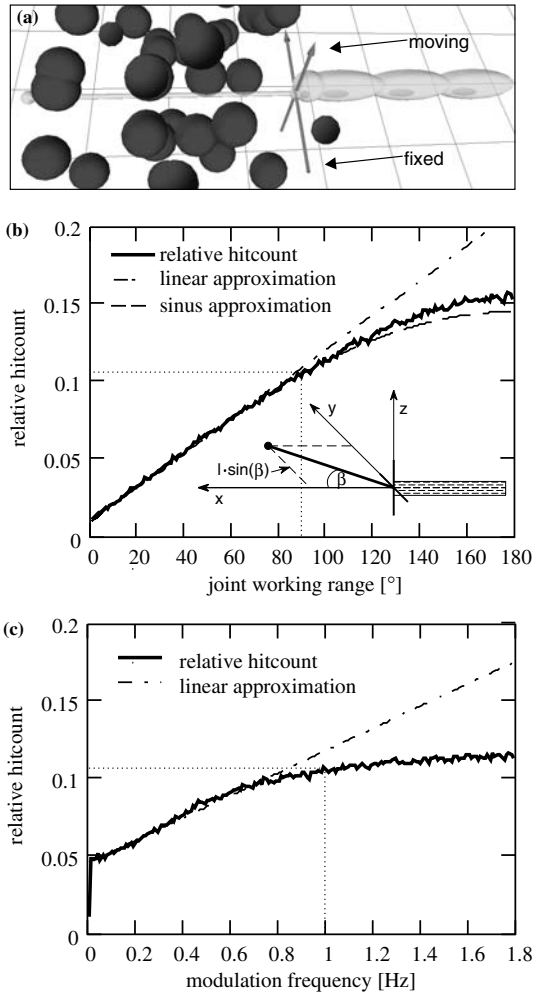

Fig. 6a–c. Tactile performance of a single-joint antenna. **a** An antenna with simple morphology was tested in a sphere environment. The first joint was fixed and the parameters of the second joint were varied. **b** Using a constant joint modulation frequency of 1 Hz, while varying the joint-action range, the relative hit count (*solid line*) increases nearly linearly (*dash-dotted line*) up to an action range of 90°. A good model for the measured dependency is a sine function (*dashed line*). **c** Using a fixed joint action range of 90°, while varying the modulation frequency the relative hit count increases linearly up to a modulation frequency of 0.8 Hz (cf. *dash-dotted line*) and saturates thereafter

Increasing the joint modulation frequency from 0 to 1.8 Hz raises the relative hit count linearly up to a frequency of 0.8 Hz. Thereafter the relative hit count slowly saturates. This is due to the fact that a further increase in antenna movement speed does not increase the likelihood of detecting new objects because they arrive too slowly. This saturation depends on the speed of the moving objects, which is equivalent to the locomotion speed of the animal in a stationary environment. The faster new objects arrive at the antenna, the later this saturation will occur. Thus, for a single-joint antenna there are threshold values of modulation frequency (1 Hz in the presented example) and action range (90°) above which further investment of energy into the movement strategy, i.e. moving the joints faster, results in only a small improvement in payoff.

3.2.2 Phase dependence. Regarding a two-joint antenna, another parameter of the movement strategy can significantly influence the relative hit count: the phase shift between the sine waves that modulate the joint angles. A systematic series of simulation experiments revealed that the phase shift has a noticeable influence on the hit count only if the joint modulation frequencies are such that the trajectory of the antennal tip is a Lissajous figure.

This influence is strongest in the case of the simplest type of Lissajous figure, with $f_\alpha = f_\beta$. For more complex figures the influence decreases. The reason for the drastic phase dependence in the case of $f_\alpha = f_\beta$ is that the phase varies the trajectory from a circular movement, sampling wide areas of the simulated environment, to a line, sampling a very small portion of it (Fig. 7). For larger frequency ratios and uneven frequency ratios, the sampled volume is nearly independent of phase shift, at least on average and when sampling for long time intervals.

3.2.3 Tactile sampling efficiency of two-joint antennae. Active movement of the antenna increases the likelihood of detecting objects. As was shown in the previous section for the single-joint antenna, there are upper bounds to this likelihood set by frequency ratio and size of the workspace. From a biological perspective, a further limit to any sampling strategy is the energy consumption caused by active movement generated by muscles. Introducing energy

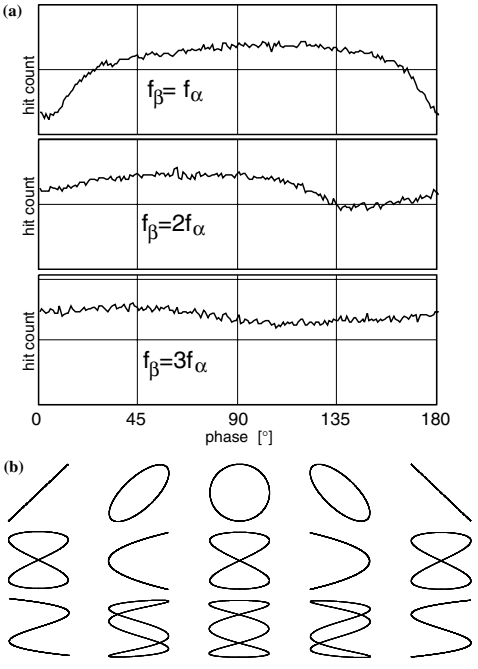

Fig. 7a, b. Influence of the phase shift on the relative hit count. If the trajectory of the antennal tip forms a Lissajous figure, the phase shift between the joint modulation frequencies f_α and f_β has a noticeable influence on the relative hit count. The relative hit count of an antenna with simple morphology tested in a sphere environment is shown. **a** If both frequencies are equal, the relative hit count strongly depends on the phase shift. For more complex Lissajous figures (e.g. for frequency ratios 1:2 and 1:3) the phase influence decreases rapidly. **b** Corresponding Lissajous figures, depicted as the frontal (YZ-)projection of the antennal tip

dependency leads to the definition of a measure of tactile sampling efficiency. Here, the tactile efficiency of an insect antenna is defined as the ratio of relative hit count by energy consumption, given a certain movement strategy and environment.

Because only very little is known about the biomechanics of insect antennae, we assume a simple model of energy consumption. Due to the small mass and, thus, inertia of the flagellum, we expect that energy consumption is proportional to the angular velocity of a joint rather than angular acceleration.

Velocity-dependent sources of energy loss can be various types of friction, including viscose friction in muscles, Coulomb friction in cuticular joint structures and drag forces acting on the long flagellum when moving through the surrounding medium. Here, friction in the joints is assumed to dominate air current friction. A simple friction model (Appendix C) is used, giving the following equation for tactile efficiency E:

$$E = \frac{\text{relative hitcount}}{k_1 f_\alpha^2 \text{range}_\alpha^2 + k_1 f_\beta^2 \text{range}_\beta^2 + k_2}, \quad (1)$$

where f_α and f_β are the joint angle modulation frequencies, range_α and range_β are the corresponding action ranges of each joint, and k_1 and k_2 are constants. Like the relative hit count, E depends on parameters of antennal morphology and movement strategy but also on the environment the antenna is moving in. Keeping the environment and antennal morphology constant, (1) can be used to generate a frequency-efficiency plot that is appropriate for evaluating different movement strategies. For example, the efficiency plot in Fig. 8 shows that the best strategy to move an antenna of the 'simple morphology' type in a sphere environment is to move both joints with the same modulation frequency and a phase offset of 90°. The resulting trajectory of the antennal tip is circular.

A comparative evaluation of the two standard morphologies and three different environments is shown in Fig. 9. The environments differ in their predominant edge orientation as the cylinders introduce a directional bias for horizontal or vertical edges (left and right columns, respectively). As a consequence, the efficiency is expected to be biased towards a preferred movement direction. This is plausible because it is more probable to hit a cylinder laterally than in its longitudinal direction. In comparison, the sphere environment has an equal distribution of edges with no directional bias. The simulation results reveal that the two morphology types behave rather differently in the tested environments: whereas for the simple morphology the most effective ratio of joint modulation frequencies depends on the selected environment, this is not the case for the *C. morosus* morphology. In the latter type, the most efficient movement strategy in all three environments is a circular movement, i.e. when both joints are moved with the same modulation frequency, $f_\alpha = f_\beta$. But if the cylinder inclination aligns with one of the joint axes of the *C. morosus* morphology, it is most efficient to move this joint faster, exactly as for the simple morphology.

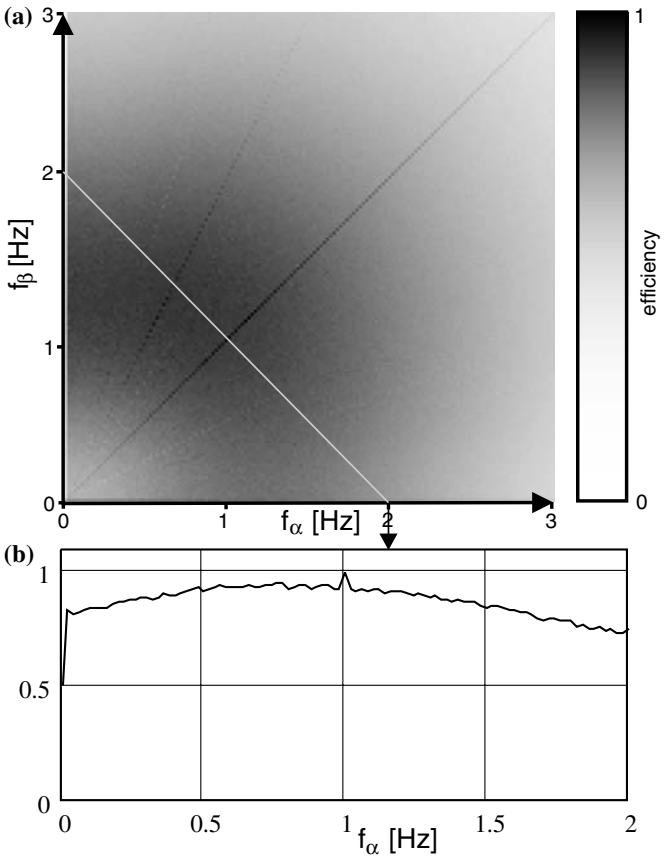

Fig. 8. a Tactile sampling efficiency of a simple antenna, moving in a sphere environment. The *greyscale* codes the efficiency value (*black maximum*) in a non-linear way, emphasizing areas of high efficiency. The maximum is centred on the *diagonal*, indicating that the most efficient movement pattern is to move the antenna with the same joint angle modulation frequency in both joints. Note that the *diagonal* is marked by a *dark ridge*. This is due to the fact that a phase shift of 90° was used, resulting in the most efficient movement pattern (Fig. 7). **b** A transect through **a**, taken along the *grey line* ($f_\alpha = q * 2\,\text{Hz}$; $f_\beta = (1-q) * 2\,\text{Hz}$; $q = [0, 1]$) reveals that efficiency decreases with an increasing frequency ratio

3.3 Asymmetries

As can be seen in Fig. 9, the introduction of a directional bias into the sampled environment causes an asymmetry in the frequency-efficiency plots, showing that, as a result of the environmental feature, the most suitable movement strategy is one where one joint moves considerably more than the other. Interestingly, such an asymmetry is also discernible in the sphere environment.

3.3.1 Asymmetry of a Cardan joint. At first glance, one would suspect the efficiency plot for an antenna with simple morphology, moving in a sphere environment (Fig. 8), to be perfectly symmetric around the diagonal formed by $f_\alpha = f_\beta$, but there is a slight asymmetry. As can be seen in the transect of Fig. 8b, where the sum of f_α and f_β is constant, generally it is more efficient to move the β joint faster than the α joint. The reason is that the effective area covered by movements of the α joint reduces with increasing β joint angle. Suppose the extreme case with

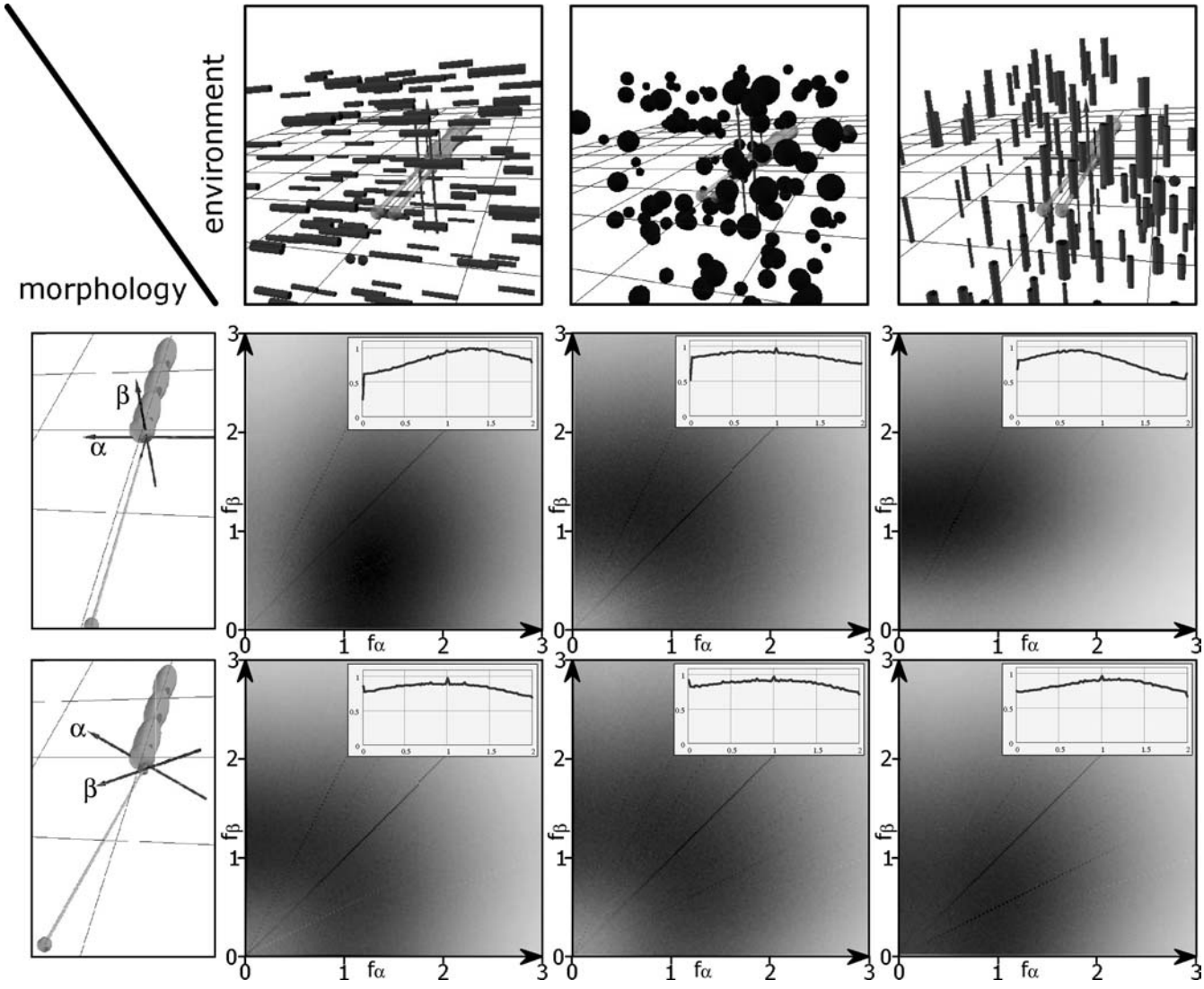

Fig. 9. Efficiency plots for two types of morphologies and three types of environments. The optimal movement strategy depends on the orientation of objects in the environment. The *middle row* shows the efficiency plots for an antenna with simple morphology. For horizontal cylinders, the maximum is located below the *diagonal*, indicating that it is more efficient to move the proximal head–scape joint (α-axis) faster than the distal scape–pedicel joint (β-axis). In the sphere environment (*middle column*) it is most efficient to move both joints with the same frequency. For vertical cylinders, it is most efficient to move the distal scape–pedicel joint faster. For the *C. morosus* morphology (*bottom row*), strategy-dependent differences in tactile efficiency are less pronounced, i.e. plots are shallower. The best movement strategy for all three environments is to move both joints with the same frequency ($f_\alpha = f_\beta$), as indicated by the diagonal ridge. *Inserts* show transects along the same line as in Fig. 8. *Greyscale* as in Fig. 8

a fixed 90° deflection of the β joint. Then, the flagellum is aligned parallel to the α-axis and active movements of the α-axis only rotate the flagellum around its long axis. In the reverse case, however, the α joint is held at an angle of 90° and the β joint moves the flagellum through an arc of up to 180°. The mathematical explanation of this asymmetric effect is that the multiplication of transformation matrices in a kinematic chain is not commutative. The mechanical explanation is that the α joint moves the β joint, even if both axes are parallel, but not vice versa. The degree of asymmetry depends on the joint action range of the beta joint. For smaller action ranges ($< 45°$), the effect diminishes.

3.3.2 Speed of progression. A further source of asymmetry in the frequency-efficiency plot is the speed of progression. So far, the simulated speed of progression, i.e. the speed of the objects flying towards the antenna, was kept constant at 50 mm/s. Yet Fig. 10 shows that speed of progression also influences the optimal choice of joint modulation frequencies. Slowing down the speed of progression causes a transition of the optimal movement strategy. Whereas at high speeds it is most efficient to move one joint faster than the other, as illustrated by the asymmetrical upper region of Fig. 10, equal frequencies may be advantageous at lower speeds. The dark vertical ridge in the middle of Fig. 10a not only marks a symmetrical lower region of the plot, it also suggests that this strategy

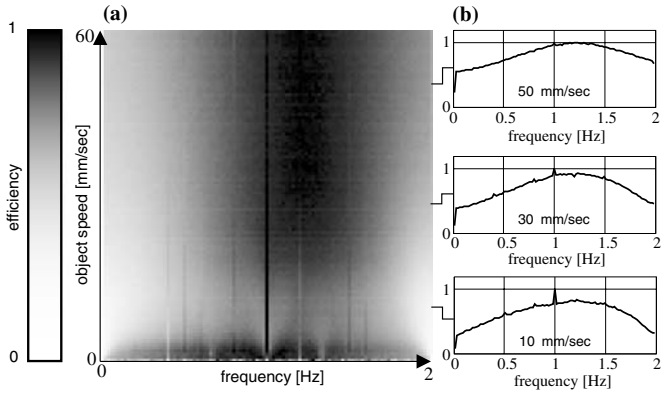

Fig. 10a, b. Tactile sampling efficiency depends on speed of progression. **a** Each *horizontal line* shows a transect from an efficiency plot calculated for an antenna with simple morphology, sampling an environment with horizontal cylinders (compare *left panel* in Fig. 9). The orientation of the transect is the same as in Fig. 8, with $f_\alpha = q \times 2$ Hz; $f_\beta = (1-q) \times 2$ Hz; $q = [0, 1]$. To simulate different speeds of progression, the speed of the cylinders was varied from 0 mm/s (*bottom*) to 60 mm/s (*top*). *Greyscale* codes tactile sampling efficiency depending on the modulation frequency ratio of the two joints (*black maximum*). Note that each line was normalised to 1 separately. **b** Selected representative cross sections of **a**. At 10 mm/s, there is a clear efficiency peak in the case of both joint frequencies. At 30 mm/s, this peak still exists, while at 50 mm/s it is preferable to move the first joint faster. Thus, the most efficient movement pattern depends not only on the structure of the environment but also on the movement speed of progression

is efficient in most situations, indicating that it may be a somewhat universally efficient movement strategy.

4 Discussion

Many insects actively move their antennae during locomotion and exploit information from antennal mechanoreceptors for course control, obstacle avoidance or tactile exploration (Staudacher et al. 2004, in press). The present theoretical study addresses three fundamental aspects of active tactile sensing. First, we use a generic model of an antenna with two hinge joints (Fig. 1) and two standard morphologies (Fig. 2) to investigate how different morphological properties affect the workspace and positioning accuracy of the antenna (Figs. 3 and 4). Second, we propose a set of simple movement strategies based on behavioural data (Fig. 5) and analyse the dependence on action range, frequency (Fig. 6) and phase (Fig. 7). Then we introduce a measure of tactile sampling efficiency and analyse its dependence on the movement strategy of the antenna (Fig. 8). Finally, we show how environmental properties such as a directional bias affects tactile efficiency (Fig. 9) and investigate two further sources of asymmetry in a preferred movement strategy: a kinematic constraint and speed dependence (Fig. 10). Below we discuss simplifications associated with the model assumptions and relate the obtained results to observations on neurobiological model organisms such as the stick insect and the cricket.

4.1 Model assumptions

The morphology of insect antennae was modelled using a simple kinematic chain with two hinge joints. The pedicel–flagellum junction was modelled as a stiff link, neglecting small deviations. The flagellum, consisting of a species-dependent number of unarticulated annuli, was modelled by a single, inflexible beam. This approach is reasonable enough for walking stick insects sampling their environment, where self-induced antennal movement without obstacle contact causes no or little deflection of the flagellum (e.g. Dürr et al. 2001). In contrast, in flying insects (e.g. locusts), bending of the flagellum is known to play an important role in detecting air currents (Gewecke and Heinzel 1980, 1987). Similarly, crayfish and lobsters may detect flagellar bending to measure water currents (Barnes et al. 2001). Moreover, obstacle contact, as it occurs during wall-following behaviour of the cockroach (Camhi and Johnson 1999), always leads to passive bending of the flagellum. However, as the main concern of the present study is to analyse the efficiency in detecting external objects, passive bending of the flagellum is of minor significance.

Sinusoidal modulation of joint angles was proposed as a simple but efficient model to move the antennal joints. Antennal trajectories recorded by Dürr et al. (2001) were used to analyse joint movements. The Fourier spectra of the corresponding joint angle trajectories suggest that more than one sine wave would give a better approximation of real antennal trajectories. Yet the dominant modes of the Fourier spectra are both widespread and fairly diverse, so more detailed data, including good dissociation of antennal and head movements, will be necessary to justify a more detailed model than the constant-frequency model used here. We are currently employing an automated, model-based video tracking software (Zakotnik et al. 2004) to analyse 3D antennal movements of unrestrained walking stick insects. This will help to reduce errors induced by manual analysis and allow sampling of large data sets that are necessary to capture the natural variability of antennal movements. Sources of such variability can be, for example, slight variations in walking speed. Because the movements of the antennae are coupled with the stepping cycle of the front legs (Dürr et al. 2001), these vary with the walking speed. Accordingly, Fourier analysis is only appropriate for short trajectories where walking speed remains approximately constant. In spite of the complexity of real antennal movements, the constant-frequency model used here provides a reasonable approximation of the cyclic movement pattern. Moreover, it allows systematic analysis of movement strategies, e.g. the impact of joint action range, modulation frequency and phase.

4.2 Tactile efficiency

In Sect. 3.2.3, the concept of tactile efficiency was defined by introducing a simple energy model for articulated insect joints. Though the energy model is hypothetical in that it assumes that energy consumption is predominantly due to friction, it incorporates a movement-dependent

cause of energy loss. Thus, tactile object detection cannot be improved ad libitum by increasing the speed of the antenna. Dependence on friction relates energy consumption to angular velocity rather than acceleration. In contrast, dependence on inertia would introduce an acceleration-dependent energy loss. Given the constant-frequency modulation of the joints, an acceleration-dependent energy loss would essentially produce the same results as a velocity-dependent one, i.e. introducing a decline of efficiency with increasing frequency and emphasising the asymmetries discussed in relation to Figs. 9, 10 and 11. As antennae are delicate and light structures (e.g. approximately 1.4 mg in *C. morosus*), inertial effects of the flagellum may be neglected.

Nevertheless, a more complex energy model will aid better understanding of different movement strategies between different insect species. Such a model will need to consider air friction and inertial and elastic properties of the joints and of the flagellum. For example, work by Gewecke and Heinzel (1980, 1987) has shown that air friction causes noticeable torques in the antennal joints of flying locusts. Similarly, we expect self-induced antennal movements to be subject to frictional forces when moving through air. However, other than in the case of a flying locust, here we assume that active antennal movements are fast compared to forward progression of the animal. Accordingly, viscous friction within the medium will depend only little on antennal posture and, thus, may be collapsed together with other sources of friction into a common measure of joint friction.

Having chosen a measure for energy loss, tactile efficiency was defined as the trade-off between the hit count and the energy consumption. Here the hit count only considers the number of intersections with randomly located objects and is, therefore, related to sampling density. This neglects the role of contact location along the flagellum. For an insect, detection distance relative to the head may be relevant in situations where reaction time is limited. The earlier objects are detected, i.e. the further away the objects are at contact time, the more time remains to adapt for ongoing movement patterns of the insect with respect to the object. Stick insects, for example, show fast re-targeting behaviour (Dürr and Krause 2001) of the front legs: antennal contact with an object often alters an ongoing swing movement of the ipsilateral front leg in such a way that the front leg tarsus touches the object. Other experiments show that stick insects with intact antennae begin to incline their body axis further away from the touched obstacle than those with cut antennae (Dürr et al. 2003). Thus, it is a clear advantage to detect objects as early as possible. In other words, distance-dependent weighting of the contact information may be necessary to evaluate species-specific movement strategies. The present study focuses on a measure of sampling density for two reasons: firstly, sampling density is independent of a species-specific requirement on contact distance that is likely to be linked to the properties such as the ratio of antennal length to leg length. Secondly, sampling density is a physical property, equivalent to the reliability to detect a given point in the environment.

It was shown in Fig. 10 that there are transitions from one favourable movement pattern to another, depending on speed of progression. Therefore, the optimal movement strategy depends not only on environmental features, e.g. on predominant edge orientation, but also on the animal's own speed within the environment. Thus, a combination of distance-weighted hit count and speed dependency will be a crucial aspect for species-specific analysis of different movement strategies.

4.3 Workspace

Another important aspect of insect antennae and tactile sensors is their workspace. This tactile action range is defined by several morphological parameters, as shown in Sect. 3.1. Tuning these morphology parameters allows for adjusting the workspace to regions of interest and, at the same time, to increase positioning accuracy. However, regions of interest and positioning accuracy are not the only factors in evolution that led to diverse antennal morphologies. Stick insects, for example, often attain a camouflage resting posture (Godden 1974), where both antennae are aligned with the body long axis to give the impression of a long stick. The need to attain such a resting position and holding it in an energy-efficient way could have been a conflicting objective in the evolution of stick insect antennae in contrast to optimising the antennal workspace in terms of acuity and overlap.

Nevertheless, the comparison of the two standard morphologies ('simple' vs. '*C. morosus*') allows us to formulate hypotheses about the tactile sensory performance of two insect species: the simple morphology is similar to the situation found in a cricket (e.g. *Gryllus campestris*), whereas the *C. morosus* morphology is that of a stick insect. Firstly, the smaller inter-axis angle of the stick insect suggests that it has better tactile angular resolution than a cricket. The cricket, on the other hand, can abduct its flagellum by 90°, i.e. to point laterally (see Honegger 1981), which a stick insect cannot do. Secondly, *C. morosus* may have axis orientations evolved in that way to sample both horizontal and vertical structures with equal efficiency (Fig. 9) while using the same movement strategy. Moreover, this strategy distributes energy equally to both joints. This could be advantageous if horizontal and vertical edges were of equal significance to a stick insect. In contrast, the orthogonal joint axes of the cricket may hint at the importance of other behavioural functions of the antennae. For example, horizontal tracking movements (Honegger 1981) are easier to control if only a single joint has to be moved, as is the case in the cricket, where the scape–pedicel joint governs this reaction.

4.4 Optimisation, evolution and design of biomimetic tactile sensors

So far, most tactile sensors employed in robotics are of passive nature and act either as simple bumpers (Brooks 1989) or as devices to estimate object locations and/or to detect walls (Cowan et al. 2003). More complex features,

such as measuring object contours (Kaneko et al. 1998) and air/water currents by measuring the bending of the sensing probe (Barnes et al. 2001), are less common.

The present study shows how active movements of insect antennae increase the sampling efficiency in their environment (Fig. 6). This will aid construction of articulated, actively movable tactile sensors for robots. By systematic variation of single parameters of morphology and movement strategy, we have shown how the tactile efficiency of the sensor can be improved, given particular environmental features. For example, Fig. 3 shows how the angle between the two joint axes can be chosen to select an appropriate combination of sampling volume, out-of-reach zones, and positioning acuity. However, the pragmatic choice of the optimal movement pattern of a technical solution will depend both on its design, i.e. its morphology, and on the environment it is moved in (e.g. Fig. 9). Therefore, application of biomimetic active tactile sensors will generally require simultaneous optimisation of movement strategy and morphology for a given environment. Multi-objective optimisation algorithms will be necessary to deal with the associated trade-offs, e.g. to balance different costs due to energy requirement, material etc. In a biological context, the present study addresses various aspects of active tactile sensors that will need to be considered to evaluate the behavioural and, thus, evolutionary significance of certain morphological and physiological properties. Just as the understanding of efficiency trade-offs will aid technical design of tactile sensors, it will likewise also aid the evaluation of species-specific or context-specific movement patterns of antennae in the light of evolutionary advantages.

Acknowledgements. This study was supported by Grant DU 380/1 of the Deutsche Forschungsgemeinschaft (DFG) to VD. The authors thank T. Bockemühl, J. Zakotnik and H. Cruse for valuable comments on earlier versions of the manuscript. The Diplomarbeit of Tamina Pinent, Bielefeld, provided the mass of the antenna.

Appendices

A Direct kinematics of an arbitrary two-joint antenna

Figure 1 shows the general kinematic model of an insect antenna with two hinge joints. The model is defined by ten scalar kinematic parameters that can be measured experimentally (e.g. Table 1): four Euler angles for axis orientations and two 3D segment vectors $\mathbf{s}_0$, $\mathbf{s}_1$. The segments connecting the joints may be of arbitrary shape, as long as they are sufficiently stiff. They can be described by their segment vector, pointing from the origin of a segment to its end. With these parameters a kinematic chain can be defined by means of concatenated homogenous rotation (**R**) - and translation matrices (**D**) in the following way:

$$\mathbf{T}(\alpha,\beta)=\mathbf{R}_z(\varphi_\alpha)\mathbf{R}_x(\psi_\alpha)\mathbf{R}_y(\alpha)\mathbf{D}_{\mathbf{s}_0}\mathbf{R}_z(\varphi_\beta)\mathbf{R}_x(\psi_\beta)\mathbf{R}_y(\beta)\mathbf{D}_{\mathbf{s}_1}\,, \quad (2)$$

Equation (2) calculates the position and orientation of the local coordinate frame of the antennal tip, **T**, given the two joint angles α and β. Multiplying the resulting matrix with $(0\ 0\ 0\ 1)^{\mathrm{T}}$ gives the position of the antenna tip relative to the base coordinate frame.

B Analytical inverse kinematics of a two-joint antenna

For the solution of the inverse kinematics problem for the generic kinematic model of Appendix A we apply the *inverse transform* method (Paul 1981). This method sequentially isolates each unknown, i.e. the joint angles, through appropriate post- or pre-multiplications of inverse transformation matrices that are part of the direct kinematics solution. Given (2) and the known position **p** of the antennal tip relative to the base frame, one needs to solve for the joint angles α and β. The local coordinate frame of the end-effector is described by the matrix

$$\mathbf{T}=\begin{pmatrix}\mathbf{x} & \mathbf{y} & \mathbf{z} & \mathbf{p}\\ 0 & 0 & 0 & 1\end{pmatrix}$$

where **x**, **y**, **z** are the unit vectors of the local frame and **p** is the origin. Here, only the position vector **p** is of interest.

Assuming a constant antennal morphology, parts of (2) can be replaced by two constant matrices **M** and **N**:

$$\mathbf{T}(\alpha,\beta)=\mathbf{M}\,\mathbf{R}_y(\alpha)\mathbf{N}\,\mathbf{R}_y(\beta)\mathbf{D}_{\mathbf{s}_1} \quad (3)$$

with constant column vectors $\mathbf{m}0,\ldots,2$, $\mathbf{n}0,\ldots,2$ and $\mathbf{s}_0$:

$$\mathbf{M}=\begin{pmatrix}\mathbf{m}0 & \mathbf{m}1 & \mathbf{m}2 & \mathbf{0}\\ 0 & 0 & 0 & 1\end{pmatrix}\quad \mathbf{N}=\begin{pmatrix}\mathbf{n}0 & \mathbf{n}1 & \mathbf{n}2 & \mathbf{s}_0\\ 0 & 0 & 0 & 1\end{pmatrix}.$$

Now **M** and $\mathbf{R}_y(\alpha)$ are moved from the right-hand side (RHS) to the left-hand side (LHS) of (3) by premultiplication with their inverses. The LHS then reads:

$$\begin{aligned}\mathrm{LHS}&=\mathbf{R}_y(\alpha)^{\mathrm{T}}\mathbf{M}^{\mathrm{T}}\mathbf{T}\\ &=\begin{pmatrix}\cdot & \cdot & \cdot & \mathbf{m}0\cdot\mathbf{p}\cos(\alpha)-\mathbf{m}1\cdot\mathbf{p}\sin(\alpha)\\ \cdot & \cdot & \cdot & \mathbf{m}1\cdot\mathbf{p}\\ \cdot & \cdot & \cdot & \mathbf{m}2\cdot\mathbf{p}\cos(\alpha)+\mathbf{m}0\cdot\mathbf{p}\sin(\alpha)\\ 0 & 0 & 0 & 1\end{pmatrix}.\end{aligned} \quad (4)$$

In (4) only the fourth column is shown, as all other columns contain orientation vectors of the local frame of the end effector. In most cases, these are unnecessary because the two degrees of freedom of the kinematic chain allow only a single orientation for a given position of the antennal tip. Exceptions are special cases where the β-axis is perpendicular to the α-axis and **p** is located on the α-axis. Then there is no unique solution to the inverse kinematics problem.

The remaining RHS reads:

$$\mathrm{RHS}=\mathbf{N}\cdot\mathbf{R}_y(\beta)\mathbf{D}_{\mathbf{s}_1}=\begin{pmatrix}\cdot & \cdot & \cdot & \xi_0(\beta)\\ \cdot & \cdot & \cdot & \xi_1(\beta)\\ \cdot & \cdot & \cdot & \xi_2(\beta)\\ 0 & 0 & 0 & 1\end{pmatrix}$$

with

$$\begin{aligned}\xi_i(\beta)\ =\ & s0_i+n1_i s1_1+(s1_0 n0_i+s1_2 n2_i)\cos(\beta)\\ &+(s1_2 n0_i-s1_0 n2_i)\sin(\beta).\end{aligned} \quad (5)$$

As the corresponding elements of the matrices LHS and RHS need to be identical, a system of three equations with two unknowns is found:

$$\mathrm{LHS} \stackrel{!}{=} \mathrm{RHS}$$

$$\begin{pmatrix} . & . & . & \mathbf{m0p}\cos(\alpha) - \mathbf{m1p}\sin(\alpha) \\ . & . & . & \mathbf{m1p} \\ . & . & . & \mathbf{m2p}\cos(\alpha) + \mathbf{m0p}\sin(\alpha) \\ 0 & 0 & 0 & 1 \end{pmatrix} = \begin{pmatrix} . & . & . & \xi_0(\beta) \\ . & . & . & \xi_1(\beta) \\ . & . & . & \xi_2(\beta) \\ 0 & 0 & 0 & 1 \end{pmatrix}.$$

The matrix elements in row two and column four and (5) form a trigonometric equation that is solvable for β:

$$c = a\cos(\beta) + b\sin(\beta) \tag{6}$$

with

$$c = \mathbf{m1} \cdot \mathbf{p} - s0_1 - n1_1 s1_1$$
$$a = s1_0 n0_1 + s1_2 n2_1$$
$$b = s1_2 n0_1 - s1_0 n2_1$$

with the two solutions:

$$\beta_{1,2} = \mathrm{atan2}(b, a) \pm \mathrm{atan2}(\sqrt{a^2 + b^2 - c^2}, c)\,. \tag{7}$$

For each β_i one can solve for α with the matrix elements in row 3 and colum 4:

$$\xi_2(\beta_i) = \mathbf{m2} \cdot \mathbf{p}\cos(\alpha) + \mathbf{m0} \cdot \mathbf{p}\sin(\alpha)\,.$$

The two solutions are:

$$\alpha_{1,2} = \mathrm{atan2}(\mathbf{m0p}, \mathbf{m2p}) \pm \mathrm{atan2}(\sqrt{(\mathbf{m0p})^2 + (\mathbf{m2p})^2 - \xi_2(\beta_i)^2}, \xi_2(\beta_i))\,. \tag{8}$$

Finally back-substitution of the introduced constants gives four pairs of solutions for $\alpha_{1,2}$ and $\beta_{1,2}$. A detailed example calculation is available as a MathCad script in the supplementary material. As (7) and (8) have two solutions for every joint angle, the appropriate ones have to be determined. For the reason stated above, typically there exists only one solution. The correct one can be found by testing the four possibilities and choosing the angle combination that results in the target point. An illustration of how the solution pairs change across the workspace of an antenna with *Carausius* morphology can also be found in the supplementary material.

C Joint friction model

A static friction model (Gaul and Nitsche 2001), i.e. the model itself does not change with velocity, with purely frictional forces is used. In such cases, the drag law by Stokes for viscous friction applies, i.e. $F_{\mathrm{drag}} \sim v$. For simplicity, static and Coulomb friction are ignored. The speed of the friction-generating movements in the joint is assumed to be proportional to the joint angle velocity. Thus, the time-varying drag force is:

$$F_{\mathrm{drag}}(t) = k_{\mathrm{drag}}\alpha'(t) = k_{\mathrm{drag}}\ \mathrm{range}_\alpha\ 2\pi f_\alpha \cos(2\pi f_\alpha t + \varphi_\alpha).$$

The drag coefficient k_{drag} describes the friction properties of the joint and depends both on mechanical construction and viscosity of muscles and tissue of the joint. For a single joint, the energy consumed during the simulation period is proportional to the integral of the time-varying drag force multiplied by the movements induced in muscles and joint structures while rotating the joint:

$$E \sim \int_{t=0}^{T} F_{\mathrm{drag}}(t)s'(t)\mathrm{d}t\,.$$

As the speed of these movements is assumed to scale linearly with joint angle velocity, their magnitude can be described by coefficient k_m:

$$s'(t) = k_m\alpha'(t).$$

Solving the integral gives:

$$E(t) = \frac{1}{2}\pi f_\alpha k_{\mathrm{drag}} k_m\ \mathrm{range}_\alpha^2 \times \left(\pi f_\alpha t + \cos(2\pi f_\alpha t + \varphi_\alpha)\sin(2\pi f_\alpha t + \varphi_\alpha) + \frac{1}{2}\varphi_\alpha\right).$$

For long simulation times t, the influence of the term cos() sin() and of the phase term diminishes and the energy consumption can be approximated by:

$$E(t) \approx k_1 f_\alpha^2\ \mathrm{range}_\alpha^2\ t$$

with

$$k_1 = \frac{1}{2}\pi^2 k_{\mathrm{drag}} k_m$$

$$\mathrm{efficiency} = \frac{\mathrm{relative\ hitcount}}{k_1 f_\alpha^2\ \mathrm{range}_\alpha^2 + k_1 f_\beta^2\ \mathrm{range}_\beta^2 + k_2}\,. \tag{9}$$

Without an additional constant k_2, the non-moving antenna ($f1 = f2 = 0$) would have infinite efficiency. k_2 thus can be interpreted as resting energy consumption and an overall cost imposed on the insect by having antennae.

References

Barnes TG, Truong TQ, Adams GG, McGruer NE (2001) Large deflection analysis of a biomimetic lobster antenna due to contact and flow. ASME J Appl Mech 68:948–951

Brooks RA (1989) A robot that walks: emergent behavior from a carefully evolved network. Neural Comput 1(2):253–262

Camhi JM, Johnson EN (1999) High-frequency steering manoeuvres mediated by tactile cues: antennal wall-following in the cockroach. J Exp Biol 202:631–643

Cowan NJ, Ma EJ, Cutkosky M, Full RJ (2003) A biologically inspired passive antenna for steering control of a running robot. In: Proceedings of the 11th international symposium on robotics research (ISRR 2003)

Dürr V, König Y, Kittmann R (2001) The antennal motor system of the stick insect *Carausius morosus*: anatomy and antennal movement pattern during walking. J Comp Physiol A 187: 131–144

Dürr V, Krause A, Schmitz J, Cruse H (2003) Neuroethological concepts and their transfer to walking machines. Int J Robot Res 22:151–167

Dürr V, Krause AF (2001) The stick insect antenna as a biological paragon for an actively moved tactile probe for obstacle detection. In: Berns K, Dillmann R (eds) Climbing and walking robots – from biology to industrial applications. In: Proceedings of the 4th international conference on climbing and walking robots (CLAWAR 2001). Professional Engineering Publishing, London, pp 87–96

Gaul L, Nitsche R (2001) Role of friction in mechanical joints. Appl Mech Rev 54(2):93–105

Gewecke M, Heinzel H-G (1980) Aerodynamic and mechanical properties of antennae as air-current sense organs in *Locusta migratoria*: I. Static characteristics. J Comp Physiol 139: 357–366

Gewecke M, Heinzel H-G (1987) Aerodynamic and mechanical properties of antennae as air-current sense organs in *Locusta migratoria*: II. Dynamic characteristics. J Comp Physiol 161: 671–680

Godden DH (1974) The physiological mechanism of catalepsy in the stick insect *Carausius morosus* br. J Comp Physiol 89: 251–274

Honegger HW (1981) A preliminary note on a new optomotor response in crickets: antennal tracking of moving targets. J Comp Physiol A 142:419–421

Horseman BG, Gebhardt MJ, Honegger H-W (1997) Involvement of the suboesophageal and thoracic ganglia in the control of antennal movements in crickets. J Comp Physiol A 181:195–204

Imms AD (1939) On the antennal musculature in insects and other arthropods. Q J Microscop Sci 81:273–320

Kaneko M, Kanayma N, Tsuji T (1998) Active antenna for contact sensing. IEEE Trans Robot Automat 14:278–291

Kindermann T (2003) Positive rückkopplung zur kontrolle komplexer kinematiken am beispiel des hexapoden laufens: experimente und simulationen. Phd Thesis, Universität Bielefeld

Land MF (1981) Optics and vision in invertebrates. In: Autrum H (ed) Handbook of sensory physiology VII/6 B comparative physiology and evolution of vision in invertebrates. Springer, Berlin Heidelberg New York, pp 471–592

Paul RP (1981) Robot manipulator: mathematics, programming and control. MIT Press, Cambridge, MA

Pelletier Y, McLeod CD (1994) Obstacle perception by insect antennae during terrestial locomotion. Physiol Entomol 19:360–362

Staudacher EM, Gebhardt M, Dürr V (2004) Antennal movements and mechanoreception: neurobiology of active tactile sensors. Adv Insect Physiol (in press)

Warrant EJ, McIntyre PD (1993) Arthropod eye design and the physical limits to spatial resolving power. Prog Neurobiol 40(4):413–461

Zakotnik J, Matheson T, Dürr V (2004) A posture optimisation algorithm for model-based motion capture of natural movement sequences. J Neurosci Meth 135(1–2):42–54

Zeil J, Sandeman R, Sandeman DC (2001) Tactile localisation: the function of active antennal movements in the crayfish *Cherax destructor*. J Comp Physiol A 157:607–617